

We are IntechOpen, the world's leading publisher of Open Access books Built by scientists, for scientists

6,900

Open access books available

186,000

International authors and editors

200M

Downloads

Our authors are among the

154

Countries delivered to

TOP 1%

most cited scientists

12.2%

Contributors from top 500 universities



WEB OF SCIENCE™

Selection of our books indexed in the Book Citation Index
in Web of Science™ Core Collection (BKCI)

Interested in publishing with us?
Contact book.department@intechopen.com

Numbers displayed above are based on latest data collected.
For more information visit www.intechopen.com



Nanofluid-Enhancing Shell and Tube Heat Exchanger Effectiveness with Modified Baffle Architecture

I Made Arsana and Ruri Agung Wahyuono

Abstract

As shell and tube heat exchanger is widely employed in various field of industries, heat exchanger design remains a constant optimization challenge to improve its performance. The heat exchanger design includes not only the architectural geometry of either the shell and tube configuration or the additional baffles but also the working fluid. The baffle design including the baffle angle and the baffle distance has been understood as key parameter controlling the overall heat exchanger effectiveness. In addition, a room of improvement is open by substituting the conventional working fluid with the nanomaterials-enriched nanofluid. The nanomaterials, e.g. Al_2O_3 , SiO_2 , TiO_2 , increases the thermal conductivity of the working fluids, and hence, the more efficient heat transfer process can be achieved. This chapter provide an insight on the performance improvement of shell and tube heat exchanger by modifying the baffle design and utilizing nanofluids.

Keywords: Design optimization, Geometry, Conductivity, Heat exchanger performance, Computational fluid dynamics

1. Introduction

Heat exchanger is considered a vital component in thermal process required in a wide range of industries. This heat exchanger is typically employed for condensation, sterilization, pasteurization, fractionation, distillation, and crystallization [1–3]. This implies that the heat exchanger shall possess an optimized design to yield the highest possible effectiveness while having a compact dimension. In general, heat transfer in a heat exchanger is substantially dominated by convection and conduction. The convection is significantly affected by the geometry of the heat exchanger and some dimensionless numbers, including Reynolds number (Re), Nusselt number (Nu) and Prandtl numbers (Pr) [1–7]. It should be noted that Re , Nu and Pr are dependent on the flow rate and fluid properties including the density, absolute viscosity, specific heat and thermal conductivity.

Practically, various heat exchangers have been developed and the shell and tube heat exchanger has been intensively employed in industries as it shows some favorable features, i.e. easy maintenance, robust construction, and higher construction reliability [8–12]. The shell and tube heat exchanger mainly comprise of shell, tubes,

front head, rear head, baffles, and nozzle. For high performance shell and tube heat exchanger, which shows high effectiveness (ϵ), several parameters affecting the heat and mass transfer process should be optimized, including the working fluid and material selection, flow rate, temperature, heat transfer rate, pressure drop, shell and tube dimension and composition, as well as baffle distance and cut, and pitch range [8–14]. Considering the architecture of heat exchanger, baffles arrangement is one of the important parameters that will increase the heat transfer and hence the effectiveness. For instance, reducing the baffle gaps could induce high pressure drop while setting the baffle gap too far could lead to less efficient heat transfer. In addition, improper baffle arrangement will lead to additional mechanical vibration which can damage the heat exchanger apparatus, and hence lower the reliability of the heat exchanger.

Other practical problem arising in industry is that the heat exchanger frequently faces unfavorable thermal properties of its working fluid, i.e. water, ethylene glycol, or oil, leading to the lower heat transfer effectiveness [14]. Therefore, it is necessary to improve the thermal properties of working fluids, one of which is by adding functional nanoparticles into the working fluid [15–17]. Recent studies have investigated the improvement of heat transfer effectiveness in nanofluids bearing various metal oxide semiconductor nanoparticles, e.g. Al_2O_3 , TiO_2 , CuO , and SiO_2 [15–26]. Among these materials, TiO_2 is one of the widely exploited nanoparticles for increasing the heat transfer effectiveness as it shows superior chemical and thermophysical stability [18–23]. Nonetheless, it should be noted that the utilization of high concentration of nanoparticles should be avoided since it may cause blockage of the fluid flow as well as induce fouling [18, 19]. Still, the use of nanoparticles in the base fluid (nanofluid) can be considered an alternative approach to improve both the thermal conductivity of the working fluid and the long-term stability by maintaining lower pressure drop in the system [20]. Some literature report that the use of nanofluids enhances the heat transfer effectiveness particularly under laminar flow condition by increasing both the concentration of nanoparticles in nanofluids and the Reynolds number [15–21]. These results suggest that the use of nanofluids increases the convection coefficient within the heat transfer process.

Considering the abovementioned facts, it is quite clear that the heat transfer process in the heat exchanger can be improved in many ways. Particularly for shell and tube heat exchanger, enhancing the heat exchanger effectiveness which is discussed in this chapter can be achieved by modifying the baffle architecture and by utilizing nanofluids with functional nanoparticles. The baffle arrangement discussed in this chapter includes the baffle distance and the baffle type which was investigated by experimental and numerical method using computational fluid dynamics (CFD). Meanwhile, the effect of nanofluid substitution to the working fluid has been investigated experimentally by varying the concentration of nanoparticles, i.e. Al_2O_3 in water and $\text{SiO}_2@\text{TiO}_2$ in water: ethylene glycol.

2. Experimental and numerical approach to evaluate the effect of baffle arrangement to the heat exchanger effectiveness

Baffle modification in this chapter includes baffle types, baffle angle and baffle distance. Modification of baffle type and angle was investigated experimentally using the experimental setup of laboratory scale of heat exchanger shown in **Figure 1** [11]. The baffle type was varied using helical and double segmental baffle, whilst the baffle angle was set in the range of 5° , 6° , and 7° . The pressure drop and the temperature difference between inlet and outlet of heat exchanger were

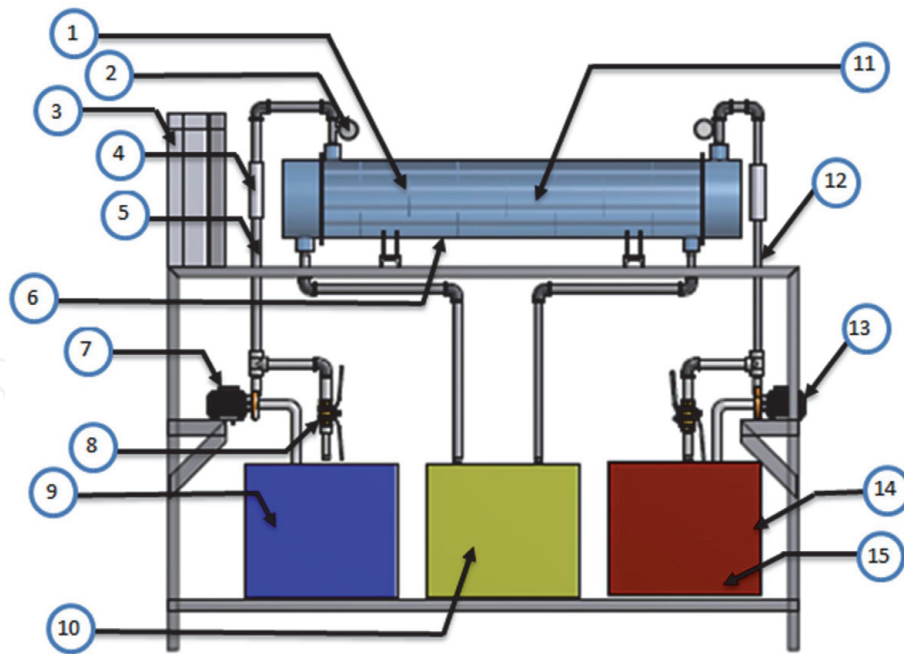


Figure 1. Schematic of heat exchanger system with modified baffle architecture: (1) baffle, (2) pressure gauge, (3) instrument box, (4) flow meter, (5) cold flow piping, (6) shell, (7) cold fluid pump, (8) valve, (9) inlet cold fluid reservoir, (10) outlet fluid reservoir, (11) tubing, (12) piping of hot fluid, (13) hot fluid pump, (14) inlet hot fluid reservoir, (15) heater. Figure was adapted from Ref. [11] with permission.

recorded to determine the heat exchanger effectiveness (*vide infra*). The experimental results here will be used for validation of the results obtained from CFD simulation and hence, the model will be further used for the heat exchanger with other modification.

To investigate the effect of baffle distance, both experimental and numerical method was used for the use of segmental and disc and doughnut baffle, respectively. Numerical method using computational fluid dynamics (CFD) was carried out as experimental approach was difficult to carry out due to the experimental complexity and high cost of experiment. For segmental baffle, the baffle distance was varied as 4, 10, and 16 cm. For numerical method, the heat exchanger dimension however followed the existing laboratory scale of heat exchanger and the baffle type was disc and doughnut baffles. The variation of baffle distances followed TEMA standards, i.e. the minimum baffle distance shall be 0.2 of the shell diameters and the maximum baffle distance shall be as large as the inner diameter of the shell. Therefore, the baffle distance was set to 30, 60, and 90 mm.

For analysis using CFD, pre-processing, solving and post-processing were employed. Pre-processing was carried out by building 3D model of the shell and tube heat exchanger using ANSYS 16.0 which was discretized (meshed) using different type of mesh types. The mesh result of was depicted in **Figure 2**. For grid independence study, the number of discretized cells spans from 1 to 3 million cells using with tetrahedral/hexahedral types. Finally, pre-processing step defined the boundary conditions summarized in **Table 1**.

The operating condition of the shell and tube heat exchanger at the boundary condition was defined as follow: Temperature of cold ($T_{c,in}$) and hot ($T_{h,in}$) fluid in the inlet was set to 80°C and of 30°C, respectively. The volumetric flow rate of hot and cold fluid was set at 4 and 6 lpm, respectively. Having defined the boundary condition, the solving stage was built by utilizing the governing equations, i.e. conservation of energy, momentum and continuity. Energy conservation was determined as follows.

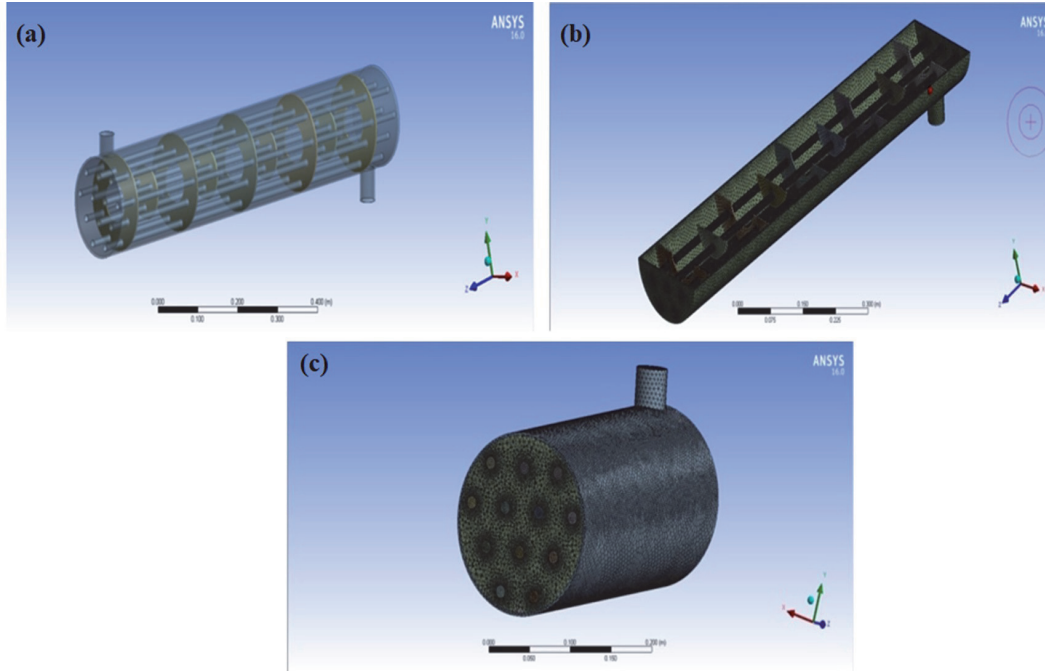


Figure 2. (a) The 3D model of shell and tube heat exchanger meshed with tetrahedral/hexahedral meshing type at different angle, and the corresponding (b) horizontal and (c) vertical cross-sectional 3D model of heat exchanger. Figures from Ref. [27] used with permission.

No.	Specification	Boundary conditions
1	Inlet	Mass flow inlet
2	Shell	Adiabatic wall
3	Tube	Convection wall
4	Baffle	Adiabatic wall
5	Outlet	Outflow

Table 1. Boundary conditions of shell and tube heat exchangers.

$$\frac{\partial}{\partial t}(\rho E) + \nabla \cdot (\vec{v}(\rho E + p)) = \nabla \cdot k_{eff} \nabla T + \nabla \cdot (\vec{\tau}_{eff} \cdot \vec{v}) + S_h \quad (1)$$

where k_{eff} is the effective conductivity which is the sum of k and k_t (thermal conductivity for the presence of turbulence). The two terms on the right side represent the energy transfer by conduction and viscosity dissipation. Meanwhile, the energy transfer was calculated as follow [17, 18]:

$$\frac{\partial}{\partial t}(\rho h) + \nabla \cdot (\vec{v} \rho h) = \nabla \cdot (k \nabla T) + S_h \quad (2)$$

where ρ was the density, h was the sensible enthalpy, k was the conductivity constant, T was the surface temperature, and S_h was the volumetric heat source. The Eq. (1) and (2) were complemented by the continuity and conservation of momentum:

$$\nabla \cdot u = 0 \quad (3)$$

$$\rho \frac{du}{dt} = F - \nabla p + \mu \nabla^2 u \quad (4)$$

where p was normal pressure (N/m^2), F was body force on solid region. For a faster convergence of numerical calculation, the Boussinesq model was considered. This model set the fluid density as a function of temperature:

$$\rho = \rho_0(1 - \beta(T - T_0)) \quad (5)$$

where β was thermal expansion coefficient ($1/\text{K}$), T_0 dan ρ_0 represented the operational parameter. This model was accurate as long as the density changes were small, or it was valid if satisfying for $\beta(T - T_0) < 1$.

The final step in CFD was the post processing stage including the data visualization in the form of a contour of static temperature, pressure, and velocity profile. Data analysis was carried out to determine the temperature distribution in the shell and tube heat exchanger with different baffle distances. The heat exchanger effectiveness (ε) was calculated in every variation of baffle distance using NTU method which considers the following steps [19]:

The rate of heat capacity (C) was calculated as

$$C_c = \dot{m}_c \times C_{p_c} \quad (6)$$

$$C_h = \dot{m}_h \times C_{p_h} \quad (7)$$

where the smallest value C_{min} considers:

$$C_{min} = > \text{If } C_h < C_c \text{ then } C_h = C_{min} \quad (8)$$

$$C_{min} = > \text{If } C_c < C_h \text{ then } C_c = C_{min} \quad (9)$$

The maximum heat transfer (q_{max}) was calculated as follow:

$$q_{max} = C_{min} \times (T_{h,in} - T_{c,in}) \quad (10)$$

$$q_{in} = q_{out} \quad (11)$$

$$q_h = q_c \quad (12)$$

$$= \dot{m}_h \times C_h \times (T_{h,in} - T_{h,out}) \quad (13)$$

$$= \dot{m}_c \times C_c \times (T_{c,out} - T_{c,in}), \quad (14)$$

and the effectiveness (ε) of the heat exchanger can then be calculated as follow:

$$\varepsilon = \frac{q_{actual}}{q_{max}} \quad (15)$$

3. Experimental approach to evaluate the effect of nanoparticles concentration in nanofluid to the heat exchanger effectiveness

The effectiveness of heat transfer using different nanofluids was assessed in the laboratory scale of experimental heat transfer system (automobile radiator training kit) which includes a closed loop of hot and cold flow (**Figure 3**). The heat exchanger was finned-tube cross flow heat exchanger (Suzuki). The nanoparticle used was Al_2O_3 and $\text{SiO}_2@\text{TiO}_2$. The $\text{SiO}_2@\text{TiO}_2$ in a mixture of EG:water (1:1 v/v) nanofluid was utilized as the hot fluid in the system. The concentration was varied in the range of 0–0.025% mass fraction of $\text{SiO}_2@\text{TiO}_2$ to EG:water base fluids. The system was functionalized with the calibrated thermocouples, flow meter and

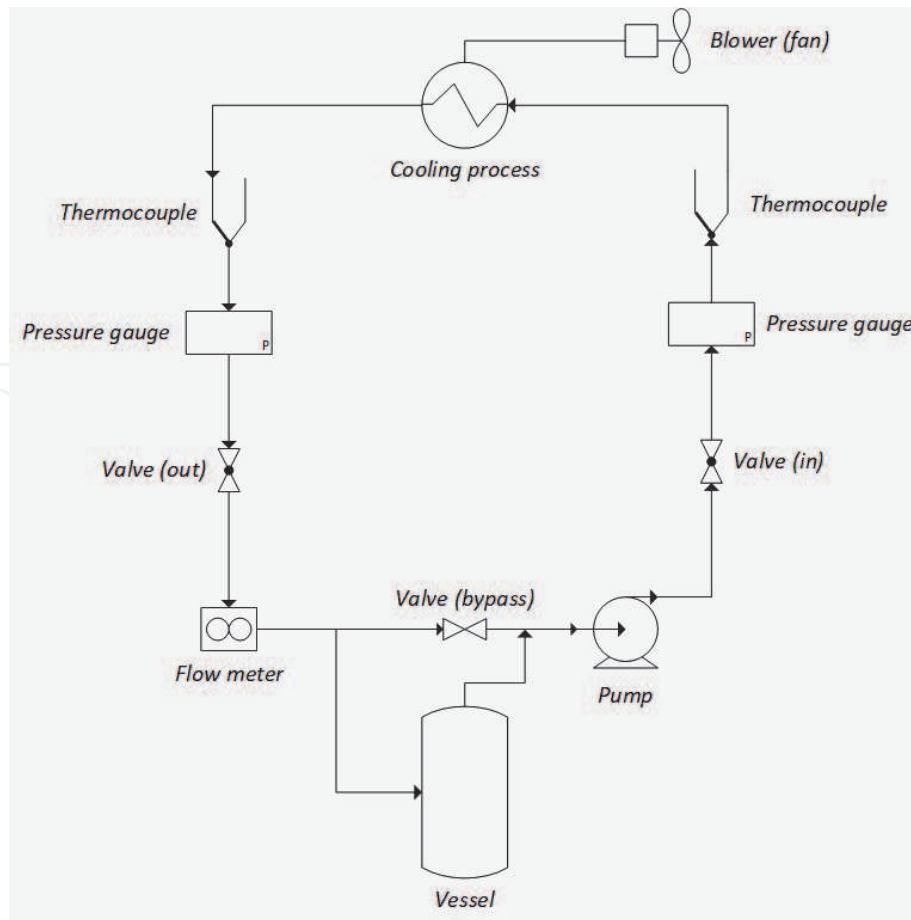


Figure 3.
The schematic of heat exchanger system for investigating the effect nanofluid concentration to its effectiveness.

pressure gauges. The schematic diagram of the automobile radiator training kit is shown in **Figure 1**.

Performance of heat exchanger using different concentration of $\text{SiO}_2@\text{TiO}_2$ was evaluated by the heat transfer effectiveness. Heat transfer parameters of nanofluids were determined by joint experimental and theoretical approach, *i.e.* only conductivity is directly determined from transient hot wire measurements. The other parameters are determined as follows:

- Density of nanofluids

$$\rho_{nf} = (1 - \phi)\rho_{bf} + \phi\rho_p \quad (16)$$

- Viscosity of nanofluids (Einstein equation)

$$\mu_{nf} = (1 + 2.5\phi)\mu_{bf} \quad (17)$$

- Reynolds number (Re)

$$\text{Re} = \frac{\rho \times V \times D_h}{\mu} \quad (18)$$

- Nusselt number (Nu) of external flow

$$Nu = 0.683 \times \text{Re}^{0.38} \times \text{Pr}^{0.37} \times \left(\frac{\text{Pr}}{\text{Pr}_s}\right)^{0.25} \quad (19)$$

- Nusselt number (Nu) of internal flow

$$Nu = 0.0265 \times Re^{0.8} Pr^{0.36} \quad (20)$$

- Convection coefficient (h_{nf}) of nanofluids

$$h_{nf} = 0.295 \left(\frac{k_w}{D_h} \right) Re^{0.64} Pr^{0.32} \left(\frac{\pi}{2} \right) \quad (21)$$

- Convection coefficient (h) of air

$$h = \frac{Nu \times k_f}{D_h} \quad (22)$$

Once all above parameters were determined, the overall heat transfer coefficient (U) was estimated. For a single tube heat exchanger, U was determined as follows:

$$U = \frac{1}{\frac{1}{h_i} + \frac{\Delta x}{k_w} + \frac{1}{h_o}} \quad (23)$$

Finally, the heat transfer rate which involves convection and conduction was evaluated by the following:

$$Q = U \times A \times \Delta T_{LMTD} \quad (24)$$

where

$$\Delta T_{LMTD} = \frac{(T_{h,in} - T_{c,out}) - (T_{h,out} - T_{c,in})}{\ln \left[\frac{(T_{h,in} - T_{c,out})}{(T_{h,out} - T_{c,in})} \right]} \quad (25)$$

4. Improvement of heat exchanger effectiveness

As previously mentioned, in this section effect of baffle architecture, including type, angle, and distance, and the nanoparticle type and concentration in nanofluids toward the heat exchange effectiveness will be discussed.

4.1 Effect of baffle arrangement

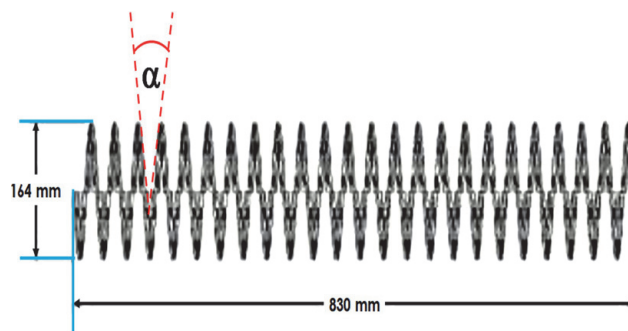
As stated in the introduction, the baffle arrangement plays significant role in the operation of heat exchanger. All thermal properties and performance of heat exchanger upon modification of baffle type, angle and distance are summarized in **Table 2**. In general, the efficiency of heat transfer process can be indicated by the temperature difference in either the hot or the cold fluid flow in the shell and tube heat exchanger, which is later used to determine the effectiveness.

Regarding the baffle selection, in this work helical and double segmental baffle were evaluated. While the baffle distance is different for both, *i.e.*, 1.64 and 1 cm for helical and double-segmental baffle, respectively, the baffle distance does not give significant effect to the performance. **Table 2** gives the experimental results and indicates that the ΔT_c for heat exchanger with helical baffles is higher than that with double segmental baffles, *i.e.*, 17.7°C vs. 14.4°C. This condition in turn yields

Baffle Modification	Parameter	ΔT ($^{\circ}\text{C}$)	ΔP (kPa)	ϵ
Baffle Type	Helical (distance: 164 mm)	17.7	7.36	0.35
	Double Segmental (distance: 100 mm)	14.4	14.48	0.30
Baffle angle ($^{\circ}$) (Helical baffle)	6	25.4	123.9	0.50
	7	21.4	88.4	0.45
	8	15.7	70.7	0.32
Baffle angle ($^{\circ}$) (Double segmental baffle)	15	24	183.4	0.48
	30	13.7	179.5	0.27
	45	4.7	178.1	0.09
Baffle Distance (cm) (Disc and doughnut baffle)	0.3	48.0	1.95	0.93
	0.6	8.0	2.98	0.20
	0.9	9.0	2.21	0.15

Table 2.

Summarized parameters in heat exchanger upon baffle modification. The data was compiled from Ref. [11, 27–29].

**Figure 4.**

The helical baffle angle (α) configuration in the shell and tube heat exchanger.

effectiveness of 0.35 which is 15% higher than the effectiveness of shell and tube heat exchanger using double segmental baffles.

As both helical and double segmental baffle show comparable performance when used in shell and tube heat exchanger, the discussion is directed to effect of baffle angle to the heat exchanger performance. The variation of the baffle angle also influences the ΔT_c . Smaller baffle angle tends to decrease ΔT_c . This is plausibly since more baffles leads to a lower heat transfer passing through the tube due to the flow disturbance by the large number of baffles (see configuration **Figure 4**). The smaller angle, it will absorb the heat faster so that the heat transfer from hot to cold fluid stream becomes less efficient. As noted in **Table 2**, the heat exchange effectiveness drops from 0.50 to 0.32 by changing the baffle angle from 5° to 7° . This trend is somewhat similar to the effect of changing double segmental baffle angle from 15° to 45° which leads to decreasing ΔT_c , ΔP and effectiveness quite significantly.

While smaller baffle angle is advantageous for heat exchanger, smaller baffle distance is also preferable for heat exchanger. This is confirmed by both experimental and numerical study. The effect of baffle distance in helical baffled shell and tube heat exchanger as assessed by computational fluid dynamics (CFD) approach shows that distancing the baffles from 30 to 90 cm decreases ΔT_c from 48.0 to 9.0 $^{\circ}$ C which results in a decreasing effectiveness from 0.93 to 0.15. The CFD results can be evaluated from the static temperature profile as displayed in **Figure 5**. As shown,

it is clear that the temperature profile of the fluid flow in the heat exchanger with a baffle distance of 30 mm is substantially different from others. The non-uniform temperature distribution is observed in the first quarter of the heat exchanger due to the turbulence flow as there are dead spaces and recirculation zones. Nonetheless, this phenomenon significantly enhances the thermo-hydraulic performance. A more uniform temperature profile in the shell side of the heat exchangers with baffle distance of 60 and 90 mm is observed. Taking a close look at the temperature distribution around the arranged tubes (Figure 5, right), significant radial distribution of temperature from the outer surface of tubes is visible for heat exchanger using 30 and 60 mm baffle distance whilst a subtle temperature changes in the surrounding the tubes is observed for heat exchanger using 90 mm-distanced baffle. At this juncture, 30 mm baffle distance is preferable for shell and tube heat exchanger design.

Other thermophysical properties of heat exchangers with a variation of the baffle distance can also be deduced from CFD, e.g. outflow temperature (T_{out}) and Nusselt number (Nu) as shown in Figure 6. The outflow temperature (T_{out}) of hot

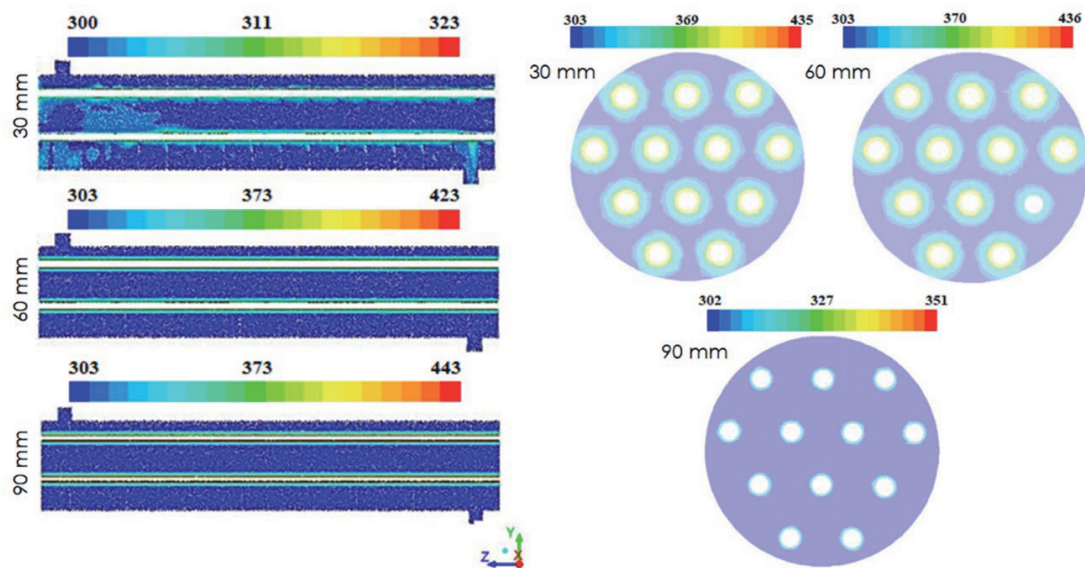


Figure 5. Cross sectional at y-axis (left) and z-axis (right) of steady state static temperature distribution in heat exchanger using 30, 60, and 90 mm baffle distance. The color code unit is K. figures from Ref. [27] used with permission.

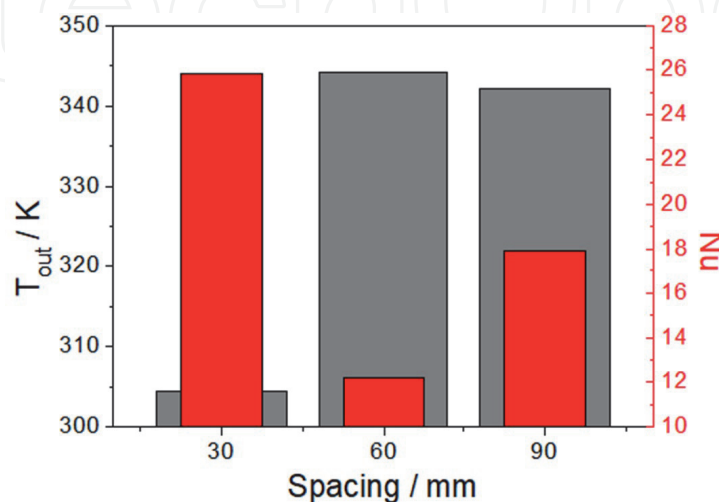


Figure 6. Thermophysical parameters deduced from numerical calculation, including outlet temperature (T_{out}), and Nusselt number (Nu).

stream is the lowest for the utilization of 30 mm-distanced baffles while heat exchanger using baffle distance of 60 and 90 mm shows T_{out} which is on par. This result indicates that the shell and tube heat exchanger with 30 mm baffle distance has the highest heat transfer from the hot to the cold fluid flow. Further, the Nusselt number displays similar trend. The highest Nu is observed for the heat exchanger using 30 mm-distanced baffles. Increasing the baffle distance from 30 mm to 60 and 90 mm lowers the Nu down to 12 and 18, respectively. It should be noted that higher Nu reflects a more efficient convection favorable in the shell and tube heat exchanger.

4.2 Effect of Nanofluids materials and concentration

It is already mentioned that the use of nanoparticles in nanofluid is to increase the conductivity of the base fluid and hence, the overall thermal transfer coefficient. Here, we used both ultra-low concentration (0.002–0.025%) and typical doping concentration (0.5–1.5%) of nanoparticles in the corresponding base fluids for the use of Al_2O_3 and core-shell $SiO_2@TiO_2$, respectively [10, 15]. In general, the heat transfer performance of nanofluids can be indirectly assessed by the dynamic of temperature changes in either the hot (T_h) or cold (T_c) fluid flow and the altered U value upon changing the nanoparticle concentration in the base fluid. These two parameters are summarized in **Table 3**.

To begin the discussion, the use of nanofluids at the lowest concentration will be first discussed. In this work, we have employed a core-shell $SiO_2@TiO_2$ nanoparticles enriched water-ethylene glycol (EG) mixture. The result show that the T_c of outflow is higher with increasing concentration of $SiO_2@TiO_2$ nanofluids. This observation indicates that the higher the concentration of nanofluids, the higher the heat is transferred as the thermal conductivity of $SiO_2@TiO_2$ increases. Furthermore, the addition of $SiO_2@TiO_2$ to the base fluid can result in an increase in the value of the convection coefficient of nanofluid as shown **Figure 7(a)**. It is also interesting to note that changing the mass fraction of $SiO_2@TiO_2$ affects the convection coefficient of the air blown to the heat exchanger due to increasing contact surface area during the heat transfer process. The addition of $SiO_2@TiO_2$ nanoparticles at a concentration of 0.025% increases the heat transfer coefficient by 9.2%.

Nanofluids	Nanoparticle concentration (% v/v)	U ($Wm^{-2} K^{-1}$)	ΔT_c ($^{\circ}C$)	ϵ
$SiO_2@TiO_2$ in Water-EG	0	22.76	11.4	0.203
	0.002	22.78	11.6	0.208
	0.008	22.82	12.8	0.218
	0.010	22.84	13.4	0.222
	0.016	22.86	15.0	0.224
	0.020	22.88	15.4	0.238
	0.025	22.90	16.9	0.246
Al_2O_3 in Water	0	29.93	10.7	0.178
	0.5	30.14	15.0	0.261
	1.0	30.19	18.4	0.350
	1.5	30.31	24.7	0.422

Table 3.

Summarized parameters of the thermal properties of nanofluids and the shell and tube heat exchanger upon the utilization of nanofluids [10, 15].

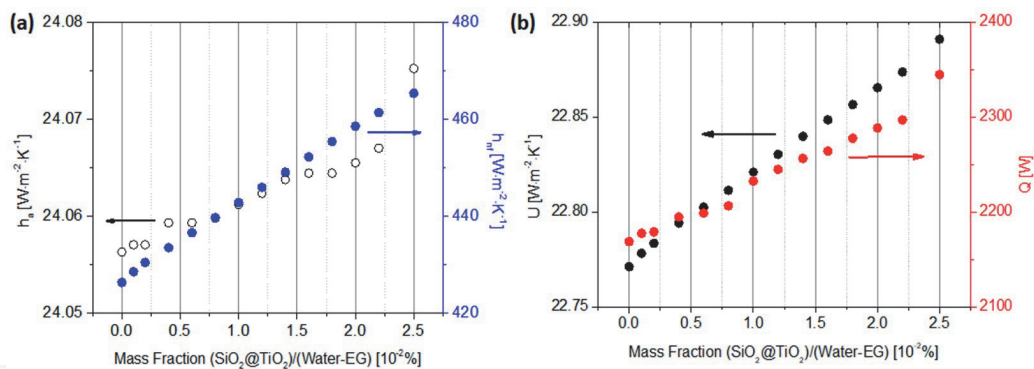


Figure 7. (a) The estimated convection coefficient of air (h_a) and $\text{SiO}_2@TiO_2$ nanofluids (h_{nf}). (b) the overall heat transfer coefficient (U) and heat rate (W) in heat exchanger using different concentration of $\text{SiO}_2@TiO_2$ nanofluids. Figures from ref. [15] used with permission.

Evaluating the total heat transfer coefficient, the results show that there is no significant increase. Only slight increase of about 0.03–0.07% is observed for each increment of mass fraction. At the same flow rate (8 liter per min) increasing the concentration of $\text{SiO}_2@TiO_2$ nanoparticles up to 0.025% yields an increasing heat transfer rate up to 18.11% (from $2168 \text{ W} \cdot \text{m}^{-2}$ to $2344 \text{ W} \cdot \text{m}^{-2}$). This heat transfer rate is higher than that of water based nanofluid containing TiO_2 nanoparticles: At a concentration of 0.25%, the heat transfer rate is only enhanced by 11% [30]. This further implies that the heat transfer rate of the low concentration $\text{SiO}_2@TiO_2$ nanofluids can be improved by increasing the flowrate of nanofluids in the heat exchanger. In general, the effectiveness of heat transfer using different $\text{SiO}_2@TiO_2$ concentration is linearly increasing with increasing the mass fraction of nanoparticles in the base fluid. It is shown that the effectiveness of heat transfer increases by 1.6–2% for increasing mass fraction by 0.005%. Overall, there is an increase in the effectiveness of heat exchanger by 21% (from 0.203 to 0.246) when the water:EG base fluid is added with 0.025% $\text{SiO}_2@TiO_2$. The results indicate that the additional nanoparticles shows better performance of heat exchanger than another study using EG:water (3:2) based nanofluid containing only 0.02% TiO_2 which shows an increase of effectiveness by 13% [22].

For higher concentration of nanoparticles, *i.e.*, Al_2O_3 in the base fluid of water shows similar trend as compared to the $\text{SiO}_2@TiO_2$ in water:EG nanofluid. Addition of merely 0.5% Al_2O_3 already increases ΔT_c by 5°C . Further increasing nanoparticles concentration from up to 1.5% results in ΔT_c of 24.7°C (*vs.* 10.7°C for pure water as working fluid). Interestingly, the U value does not change significantly as also observed for $\text{SiO}_2@TiO_2$ in water:EG nanofluid. The U value for base fluid of water is known $29.93 \text{ W} \cdot \text{m}^{-2} \cdot \text{K}^{-1}$ while the deployment of Al_2O_3 up to 1.5% volume fraction only improves U value up to $30.31 \text{ W} \cdot \text{m}^{-2} \cdot \text{K}^{-1}$. Of course, the observed effects in the Al_2O_3 -water nanofluid can be explained by the same phenomena as previously discussed in the $\text{SiO}_2@TiO_2$ in water:EG nanofluid.

5. Conclusion

In this chapter, we have shown that improvement of shell and tube heat exchanger effectiveness can be achieved by optimizing the baffle architecture and by using nanofluids to substitute the conventional working fluid. We have investigated the effect of baffle type and baffle distance in the laboratory scale of shell and tube heat exchanger using experimental and numerical approach, respectively. In

general, the heat exchanger effectiveness is affected by the baffle arrangement and type. It is found that helical baffle is preferable than double segmental baffle which yields 15% higher effectiveness. Larger baffle separation distance consistently shows a significantly decreasing heat transfer rate as indicated by lower ΔT . This in turn lowers the heat exchanger effectiveness quite substantially. In addition, angle also quite essential to optimize. For the utilization of helical baffle, only changing 5° to 7° already lowers the effectiveness from 0.50 down to 0.32.

The utilization of nanofluid has been demonstrated to enhance the heat transfer process yielding higher effectiveness. Even at the extremely low concentration of nanoparticles, *i.e.*, 0.002 to 0.025%, the water-ethylene glycol based nanofluids containing $\text{SiO}_2@\text{TiO}_2$ core-shell nanoparticles enable enhancement of heat exchanger effectiveness by 20%. This finding is essential as it is not necessary to use high concentration of nanoparticles to improve heat exchanger effectiveness while avoiding fouling inside the tubing system of shell and tube heat exchanger. Another set of examples has been shown that using water based working fluid using Al_2O_3 . Increasing volume fraction of Al_2O_3 nanoparticles significantly boosts the effectiveness up to 0.422 which is plausibly a result of increasing thermal conductivity of the water base fluid.

Acknowledgements

Financial support by the Center of Research and Development (*Lembaga Penelitian dan Pengabdian Kepada Masyarakat*) of Universitas Negeri Surabaya and the directorate of research and community development (*Direktorat Riset dan Pengabdian Kepada Masyarakat*) of Institut Teknologi Sepuluh Nopember is highly acknowledged. Authors also would like to thank to the Mechanical Engineering Department and Heat Transfer Laboratory of Universitas Negeri Surabaya for their technical support.

Conflict of interest

Authors declare that there is no conflict of interest.

Nomenclature

C_c, C_h	Heat capacity of hot and cold fluid, $\text{W}/^\circ\text{C}$
\dot{m}_h, \dot{m}_c	mass flow rate, kg/s
$C_{p,h}, C_{p,c}$	Specific heat of hot and cold fluid, $\text{J}/\text{kg } ^\circ\text{C}$
h	Enthalpy, $\text{J}/\text{kg } ^\circ\text{C}$
q_{max}	Maximum heat transfer (W)
q_{actual}	Actual heat transfer (W)
T	Temperature, $^\circ\text{C}$ or K
u	Velocity of the medium, m/sec .
V	Volume, m^3
ε	heat exchanger effectiveness, n.d

Subscripts

h, c	Refers to hot and cold fluid
i, o	Refers to inflows and outflows

Greek symbols

β	Extinction or attenuation coefficient, m^{-1}
θ	Polar or cone angle measured from normal of surface, rad.
ρ_f	Density of a fluid. kg/m^3
σ_{scat}	Scattering coefficient, m^{-1}
σ_{abs}	Scattering coefficient, m^{-1}
ϕ	Azimuthal angle, rad.
Φ	Scattering phase function
Ω	Solid angle, sr

Author details

I Made Arsana^{1*} and Ruri Agung Wahyuono²

¹ Department of Mechanical Engineering, Faculty of Engineering, Universitas Negeri Surabaya, Surabaya, East Java, Indonesia

² Department of Engineering Physics, Faculty of Industrial Technology and System Engineering, Institut Teknologi Sepuluh Nopember, Surabaya, Indonesia

*Address all correspondence to: madearsana@unesa.ac.id

IntechOpen

© 2021 The Author(s). Licensee IntechOpen. This chapter is distributed under the terms of the Creative Commons Attribution License (<http://creativecommons.org/licenses/by/3.0>), which permits unrestricted use, distribution, and reproduction in any medium, provided the original work is properly cited. 

References

- [1] Mazubert A, Fletcher DF, Poux M, Aubin J. Hydrodynamics and mixing in continuous oscillatory flow reactors – Part I: Effect of baffle geometry. *Chem. Eng. Process.: Process Intensification* 2016; 108; 78–92. DOI:10.1016/j.cep.2016.07.015
- [2] Akbar FR, Arsana IM. Effect of Wire Pitch on Capacity of Single Staggered Wire and Tube Heat Exchanger Using Computational Fluid Dynamic Simulation. *International Journal of Engineering*. 2020;33;1637–1642. DOI: 10.5829/ije.2020.33.08b.22
- [3] Arsana IM, Susianto, Budhikarjono K, Altway A. Optimization of The Single Staggered Wire and Tube Heat Exchanger. *MATEC Web of Conferences*. 2016;58; 01017. DOI: 10.1051/mateconf/20165801017
- [4] Javaran EJ, Nassab SAG, Jafari S. Numerical Simulation of a Three-Layered Radiant Porous Heat Exchanger Including Lattice Boltzmann Simulation of Fluid Flow. *International Journal of Engineering Transaction A: Basics*. 2011; 24; 301–319. DOI:10.5829/idosi.ije.2011.24.03a.09
- [5] He X, Zhao H, Chen X, Luo Z, Miao Y. Hydrodynamic Performance Analysis of the ducted propeller Based on the Combination of Multi-Block Hybrid Mesh and Reynolds Stress Model. *Journal of flow control, Measurement, and Visualization*. 2015; 3; 67–74. DOI:10.4236/jfcmv.2015.32007
- [6] Assari MR, Tabrizi HB, Parvar M, Farhani MA. Experimental Investigation of Sinusoidal Tube in Triplex-Tube Heat Exchanger during Charging and Discharging Processes Using Phase Change Materials. *International Journal of Engineering Transactions A: Basics*. 2019; 31(7); 999–1009. DOI:10.5829/ije.2019.32.07a.13
- [7] Maurya RS, Singh S. Numerical Investigation of Isothermal Flow Around. Impingement Plates in a Shell and Tube Heat Exchanger. *Journal of Thermal Engineering*. 2017; 3(5);1442–1452. DOI:10.18186/journal-of-thermal-engineering.338901
- [8] Singh G, Nandan A. Experimental Study of Heat Transfer Rate in a Shell and Tube Heat Exchanger with Air Bubble Injection (technical note). *International Journal of Engineering Transactions B: Application*. 2016; 29(8); 1160–1166. doi: 10.5829/idosi.ije.2016.29.08b.16
- [9] Thakur G, Singh G, Thakur M, Kajla S. An experimental study of nanofluids Operated Shell and Tube Heat Exchanger with Air Bubble Injection. *International Journal of Engineering Transaction A: Basics*. 2018; 31; 136–143. DOI: 10.5829/ije.2018.31.01a.19
- [10] Arsana IM, Agista DR, Ansori A, Sutjahjo DH, Effendy M. The Effect of Nanofluid Volume Fraction to The Rate of Heat Transfer Convection Nanofluid Water- Al_2O_3 on Shell and Tube Heat Exchanger. *Journal of Physics: Conference Series*. 2020;1569;032048. DOI: 10.1088/1742-6596/1569/3/032048
- [11] Arsana IM, Rasyid AHA, Drastiawati NS, Ariyanto SR. The Influence of Baffle Gap to The Effectiveness of Shell and Tube Heat Exchanger with Helical Baffle. *Journal of Physics: Conference Series*. 2020;1569; 042091. DOI: 10.1088/1742-6596/1569/4/042091.
- [12] Lei Y, Li Y, Jing S, Song C, Lyu Y, Wang F. Design and performance analysis of the novel shell-and-tube heat exchangers with lower baffles. *Appl. Thermal Eng.* 2017; 125: 870–879. DOI: 10.1016/j.applthermaleng.2017.07.081
- [13] Sreedhar V, Chandra GR, Kanth TNR, Somaiah A. Experimental

Investigation on Shell and Tube heat Exchanger Using Segmental and Disc-Doughnut Type Baffles. *Int. J. Mechanical Engineering and Technol.* 2017; 8(12): 975–984.

[14] Sarkar S, Singh KK, Shenoy KT. CFD Modeling of Pulsed Disc and Doughnut Column: Prediction of Axial Dispersion in Pulsatile Liquid-Liquid Two-Phase Flow. *Ind. Eng. Chem. Res.* 2019; 58(33); 15307–15320. <https://doi.org/10.1021/acs.iecr.9b01465>

[15] Arsana IM, Muhimmah LC, Nugroho G, Wahyuono RA. Enhanced Heat Transfer Effectiveness Using Low Concentration SiO₂-TiO₂ Core-Shell Nanofluid in a Water/Ethylene Glycol Mixture. *Journal of Engineering Physics and Thermophysics.* 2021; 94(2); 439-446.

[16] Rusu MM, Wahyuono RA, Fort CI, Dellith A, Dellith J, Ignaszak A, Vulpoi A, Danciu V, Dietzek B, Baia L. Impact of drying procedure on the morphology and structure of TiO₂ xerogels and the performance of dye-sensitized solar cells. *J. Sol-Gel Sci. Technol.* 2017; 81(3); 693–703.

[17] Ebrahimnia-Bajestan E, Moghadam MC, Niazmand H, Daungthongsuk W, Wongwises S. Experimental and numerical investigation of nanofluids heat transfer characteristics for application in solar heat exchangers. *International Journal of Heat Mass Transfer.* 2016; 92; 1041–1052.

[18] Davarnejad R, Kheiri M. Numerical Comparison of Turbulent Heat Transfer and Flow Characteristics of SiO₂/Water Nanofluid within Helically Corrugated Tubes and Plain Tube. *International Journal of Engineering, Transaction B: Applications.* 2015; 28; 1408–1414.

[19] Duangthongsuk W, Wongwises S. Measurement of temperature-dependent thermal conductivity and

viscosity of TiO₂-water nanofluids. *Experimental Thermal Fluid Science.* 2009; 33; 706–714.

[20] Barzegarian R, Moraveji MK, Aloueyan A. Experimental investigation on heat transfer characteristics and pressure drop of BPHE (brazed plate heat exchanger) using TiO₂-water nanofluid. *Experimental Thermal Fluid Science.* 2016; 74; 11–18.

[21] Azmi WH, Hamid KA, Mamat R, Sharma KV, Mohamad MS. Effects of working temperature on thermo-physical properties and forced convection heat transfer of TiO₂ nanofluids in water – ethylene glycol mixture. *Applied Thermal Engineering.* 2016; 106; 1190–1199.

[22] Reddy MCS, Rao VV. Experimental studies on thermal conductivity of blends of ethylene glycol-water-based TiO₂ nanofluid. *International Community Heat Mass Transfer.* 2013; 46; 31–36.

[23] Bhanvase BA, Sarode MR, Putterwar LA, Abdullah KA, Deosarkar MP, Sonawane SH. Intensification of convective heat transfer in water/ethylene glycol based nanofluids containing TiO₂ nanoparticles. *Chemical Engineering Process.* 2014; 82; 123–131.

[24] Hamid KA, Azmi WH, Mamat R, Sharma KV. Experimental investigation on heat transfer performance of TiO₂ nanofluids in water-ethylene glycol mixture, *International Community Heat Mass Transfer.* 2016; 73; 16–24.

[25] Davarnejad R, Ardehali RM. Modeling of TiO₂-water Nanofluid Effect on Heat Transfer and Pressure Drop, *International Journal of Engineering, Transaction B: Applications.* 2014; 27; 195–202.

[26] Pirhayati M, Akhavan-Behabadi MA, Khayat M. Convective Heat

Transfer of Oil based Nanofluid Flow inside a Circular Tube, International Journal of Engineering, Transaction B: Applications. 2014; 27; 341–348.

[27] Arsana IM, Wiyanto T, Wijanarko DV, Soeryanto, Wahyuono RA, Numerical Investigation on The Performance of Shell and Tube Heat Exchanger with Modified Disc and Doughnut Baffle Distance. (submitted)

[28] Arsana IM, Setyawan R. Simulation Study on Effect of Baffle Angle to the Heat Exchanger Effectiveness on Shell and Tube Heat Exchanger Using Helical Baffle. (submitted)

[29] Nada QA, Arsana IM, Study on New-Orientation of Baffle in Shell and Tube Heat Exchanger using Double Segmental Baffle. (submitted)

[30] Eiamsa-ard SK, Kiatkittipong K, Jedsadaratanachai W. Heat Transfer Enhancement of TiO_2 /Water Nanofluid in A Heat Exchanger Tube Equipped with Overlapped Dual Twisted-tapes. Engineering Science and Technology, an International Journal. 2015; 18; 336–350.